ELSEVIER

Chemical Engineering Science 62 (2007) 793–804

Chemical Engineering Science

www.elsevier.com/locate/ces

Scaling-up from first principles of a photocatalytic reactor for air pollution remediation

Gustavo E. Imoberdorf, Horacio A. Irazoqui, Orlando M. Alfano*, Alberto E. Cassano

INTEC, Instituto de Desarrollo Tecnológico para la Industria Química, Universidad Nacional del Litoral and CONICET, Güemes 3450, S3000GLM Santa Fe, Argentina

Received 27 April 2006; received in revised form 3 October 2006; accepted 9 October 2006
Available online 17 October 2006

Abstract

A proposal for scaling-up photocatalytic reactors is described and applied to catalytic walls coated with a thin layer of titanium dioxide and irradiated with near UV radiation. The method is exclusively based on the fundamentals of chemical reaction engineering and radiative transfer theory, without the use of adjustable parameters in going from the laboratory information to a pilot scale apparatus. Mathematical modeling has been utilized. From kinetic information obtained in experiments performed in a flat plate of 81 cm^2, operating at steady state in a continuous, well-mixed reactor with recycle, predictions for a continuous flow, multi-annular reactor having a catalytic surface of 5209 cm^2 agree very well with the validation tests. Thus, the achieved scale-up implies a change in size, shape, configuration and operating conditions of both employed reactors. Requirements to apply satisfactorily the proposed methodology are reported in detail. The root mean square error in the verification of conversion predictions for the larger scale photocatalytic reactor when compared with experimental data is less than 5.6%.

Keywords: Scaling-up; Photocatalysis; Laboratory reactor; Pilot-scale reactor; Air pollution remediation; Perchloroethylene

1. Introduction

Remediation of water or air having low concentrations of a wide family of pollutants have been traditionally accomplished using absorption with granulated activated carbon (GAC) as a feasible polishing method for low-polarity hydrocarbons; however, this technology does not work well for halogenated hydrocarbons, which constitute an important fraction of contaminants. In some cases air stripping is also used for water restoration because of its low treatment cost and its attributes of simplicity and flexibility, but is not practical for low vapor pressure compounds, has some limitations when the objective is an extremely high level of removal of impurities and is not functional for gaseous systems. In any event, none of these approaches leads to the destruction of the undesirable compounds but simply translate them to a less endangering place.

This is problematic in that regulatory standards have become increasingly stringent. Augmenting demands in the results of polishing techniques to attain high contaminant removal rates has lead to a significant research and development activity in the area of advanced oxidation technologies (AOTs) that provide very high levels of destruction for almost all organic compounds, including chlorinated compounds. Among the various types of AOTs, heterogeneous photocatalytic techniques have been the subject of appreciable research efforts for these applications, due to their capabilities for complete destruction of a very wide range of hazardous contaminants and completeness of degradation to innocuous products.

Heterogeneous photocatalysis employs semiconductors such as TiO_2 that coming in contact with the appropriate wavelength of UV radiation results in the formation of electron–hole pairs that initiate low selectivity, oxidation reactions of the contaminant species that often lead to harmless products such a carbon dioxide, water and inorganic acids. TiO_2 is a wide band-gap semiconductor and absorbs near-UV and shorter wavelengths of the electromagnetic spectrum; moreover, TiO_2 has been

* Corresponding author. Tel.: +54 342 451 1546/47; fax: +54 342 451 1087.
E-mail address: alfano@intec.unl.edu.ar (O.M. Alfano).

0009-2509/$ - see front matter © 2006 Elsevier Ltd. All rights reserved.
doi:10.1016/j.ces.2006.10.004

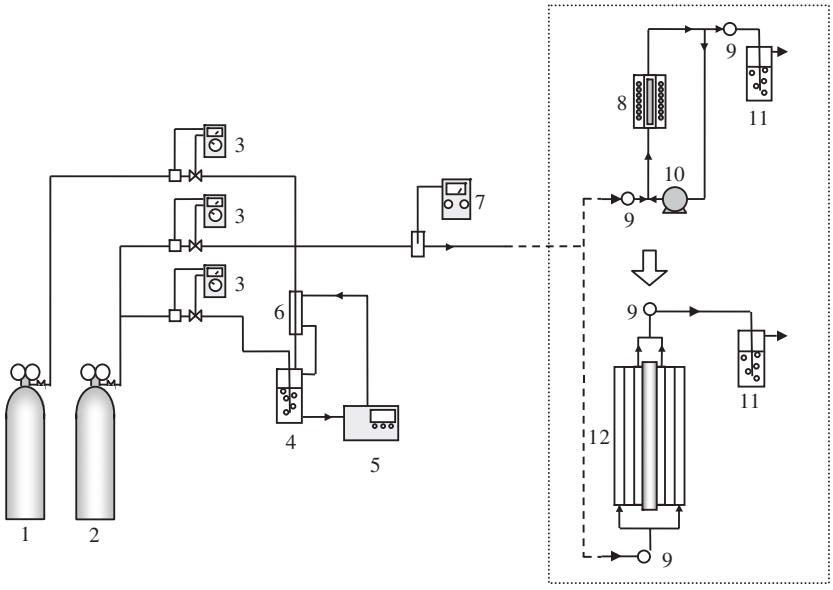

Fig. 1. Flow sheet of the experimental devices. Laboratory and pilot-scale photoreactors. Keys: (1) PCE + air, (2) air, (3) mass flowmeter, (4) air humidifier, (5) thermostatic bath, (6) heat exchanger, (7) thermohygrometer, (8) flat plate photoreactor, (9) sampling device, (10) recycle pump, (11) gas scrubber, and (12) multi-annular photocatalytic reactor.

preferred in these applications because is non toxic, abundant, low-priced, and resists photo-corrosion (Hoffmann et al., 1995).

Photocatalytic reactions with suspended solid particles have been extensively studied and are known to render the highest activity in the vast majority of cases but do not provide simple, practicable technical solutions for air pollution remediation. Immobilized catalyst configurations in the form of packed bed, membrane, monolith or catalytic wall reactors have been the prevalent proposals (Raupp et al., 1997; Hall et al., 1998; Nicolella and Rovatti, 1998; Hossain et al., 1999; Zhang et al., 2003; Ibrahim and De Lasa, 2004; Chang et al., 2005; Esterkin et al., 2005; Mohseni, 2005).

One of the difficulties for the expanded use of these technologies is the lack of reliable and validated methods to design the appropriate reactors and, much more important, to reach the desired results circumventing the requisite to resorting to expensive, progressively senlarging empirical developments (upscaling steps) to move from laboratory results to the required commercial scale.

The point is that knowing a fairly complete reaction scheme (or even better, a mechanism) of the chemical process, and a comprehensive representation of the effects of the different variables to describe the reaction rate independently of the shape and configuration of the laboratory reactor, applying the fundamentals of chemical reaction engineering and radiation transport, the design of the large scale apparatus can be made directly from laboratory experiments. This is more easily reachable because of two special features of photochemical and, particularly, photocatalytic processes: (i) due to the high radiation absorption properties of titanium dioxide, the optical path length of the characteristic dimension (the main direction of radiation propagation) of the commercial reactor will never be very much larger than the one that should be employed in a well-designed laboratory reactor and (ii) unless the process scale is so large and the equipment investment is so important that an agreement can be reached with the lamp manufacturers for special lamps' specifications (size, shape and wavelength and power emission), the design and, consequently, the size of a feasible reactor, is very much constrained by the commercial availability of the radiation sources; i.e., the design can be made in the predictive simulation mode of the large reactor scale configuration, based on almost predefined optical path lengths and available lamp dimensions and output powers.

It is the purpose of this work to show a procedure for an a priori design of a pilot scale, catalytic wall, continuous multi-annular photoreactor from information obtained in a small laboratory reactor of very different size, shape and configuration; i.e., a proposal for a design from first principles of commercial scale photocatalytic reactors (Fig. 1).

2. Methodology

The essential target is to obtain from the laboratory reactor an intrinsic reaction kinetics for the proposed reaction. This objective is more easily achieved when a reaction mechanism, or even less, just a plausible and veritable representative reaction scheme is known. The less phenomenological, i.e., derived from dependable reaction paths the kinetics is, the more reliable will be the results. In this aspect the contribution from fundamental chemistry research is very valuable.

The second point at issue is to employ the same catalyst preparation protocol and morphology in both reactors, and provide the possibility that the laboratory reactor be rigorously

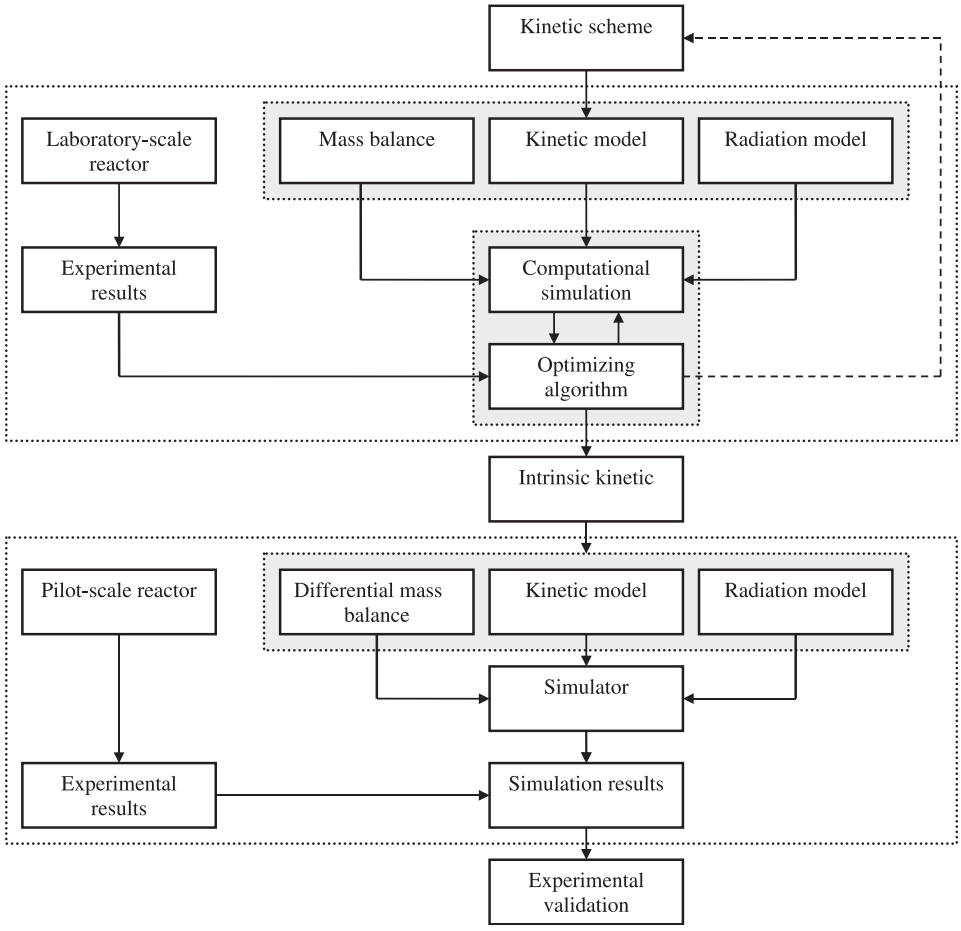

Fig. 2. Up-scaling methodology diagram.

modeled. To some extent the last part of this condition implies to use a laboratory device as simple as possible, usually custom made and, even if it is desired to work at different temperatures, operate the reactor under isothermal conditions. A very important requisite is that the experimental results should be totally free of mass transfer limitations; i.e., to operate the reactor in the kinetic control regime.

As shown in Fig. 2, from the reaction scheme (a series of intermediate reactions starting from the photocatalyst activation and proceeding to the transformation of reactants into products) the first step is to derive a reaction kinetics mathematical model that in general terms must always be of local value because of the usually irreducible non uniformities of the existing radiation field. It may depend on the intervening stable species local concentrations, the catalyst loading and/or specific surface area and the local value of radiation absorption rate. In this expression, none of the reactor characteristics can be included. Even more, this kinetic expression (the reaction rate) could be of local value, sometimes depending on position and/or time. This general statement does not exclude the possibility that as a particular case, a carefully planned laboratory reactor could render a reaction kinetic expression that is independent of time and valid for the whole reactor with no spatial dependence whatsoever, as long as the method employed to obtain its parameters permits to safely extrapolate the result to more complex situations. This is the case that will be shown in this work.

The above objective is possible resorting to precisely posed mathematical models for the laboratory reactor, derived from accurate mass balances and the radiation transport equation. Thus, employing the radiative transfer model to describe the radiation field inside the reactor, it is possible to incorporate the local value of the photon absorption rate by the catalyst in the kinetic expression and supply the complete, point valued result of the reaction kinetics into a local macroscopic mass balance depending upon the case. In this way the laboratory reactor can be precisely simulated and used to extract the intrinsic kinetics parameters of the reaction model with a non linear, multiparameter estimator rendering a final expression that must be an exclusive function of the reaction variables.

Advancing to the change of scale, the same kinetic model for the reaction obtained in the laboratory experiments must be used with the exception that the photon absorption rate must be calculated from a different radiation balance derived for the larger reactor. For this reason, it should not be unexpected that

the mass and radiation balances will almost always be very different responding to the new proposed, large scale reactor size, shape, configuration and operation. The radiation transfer equation must be applied to the new reactor in order to predict the local photon absorption rate in a reaction space that generally will be of dissimilar size and shape and irradiated with a different size and/or shape of lamp. Again, the resulting expression must be inserted in the mass balance and, operating the simulator in the predictive mode to calculate the reactor output variables. In this work, to validate the proposed methodology, these results will be compared with experiments performed in a pilot scale reactor.

3. Laboratory photocatalytic reactor

3.1. Summary of reactor description and model

As it is sketched in Fig. 3, the laboratory photocatalytic reactor consists of: (i) a rectangular plate of glass transparent to the useful wavelength range of the applied radiation, having a 4.5 × 9 cm size, coated with a thin layer of titanium dioxide on both sides, (ii) two reaction chambers, each one of them confined between the borosilicate glass plate and a rectangular acrylic window transparent to the employed UV radiation, and (iii) two sets of seven black-light lamps (Philips TL 4W/08 F4T5/BLB), each set positioned on either side of the glass plate. A thin layer of TiO_2 was deposited on each surface of the glass plate using a variation of a previously proposed sol–gel technique (Yamazaki-Nishida et al., 1993). The laboratory photoreactor dimensions and characteristics are shown in Table 1. More details concerning the reactor operation and analytical procedures can be found elsewhere (Imoberdorf et al., 2005).

The chosen reactor operation permits a very simple modeling for the species conservation equation. A macroscopic mass balance for the model pollutant (PCE) in the whole continuous, with recirculation, well-mixed, steady state photoreactor (Fig. 1), gives:

$$\langle r_{\mathrm{PCE}}\rangle_{A_R} = \frac{Q^{\mathrm{in}}(\langle C_{\mathrm{PCE}}\rangle^{\mathrm{out}} - \langle C_{\mathrm{PCE}}\rangle^{\mathrm{in}})}{A_R}. \quad (1)$$

Here, $\langle r_{\mathrm{PCE}}\rangle_{A_R}$ is the reactor catalytic surface area averaged reaction rate, Q^{in} is the volumetric flow rate of the recycle inlet stream, A_R the reaction area of the photocatalytic plate, and $\langle C_{\mathrm{PCE}}\rangle^{\mathrm{in}}$ and $\langle C_{\mathrm{PCE}}\rangle^{\mathrm{out}}$ the averaged pollutant concentrations at the inlet and outlet streams of the recycle, respectively. Note that Eq. (1) allows us to obtain the experimental PCE reaction rate from easily measurable variables.

It should be noted that the reaction rate (r_{PCE}) can be a function of position (x, y) on the reacting plate. Consequently, the reaction rate averaged over the reacting surface area can be obtained from:

$$\langle r_{\mathrm{PCE}}\rangle_{A_R} = \frac{1}{A_R}\int_{x=0}^{x=Xr}\int_{z=0}^{z=Zr} r_{\mathrm{PCE}}(x,z)\,\mathrm{d}z\,\mathrm{d}x. \quad (2)$$

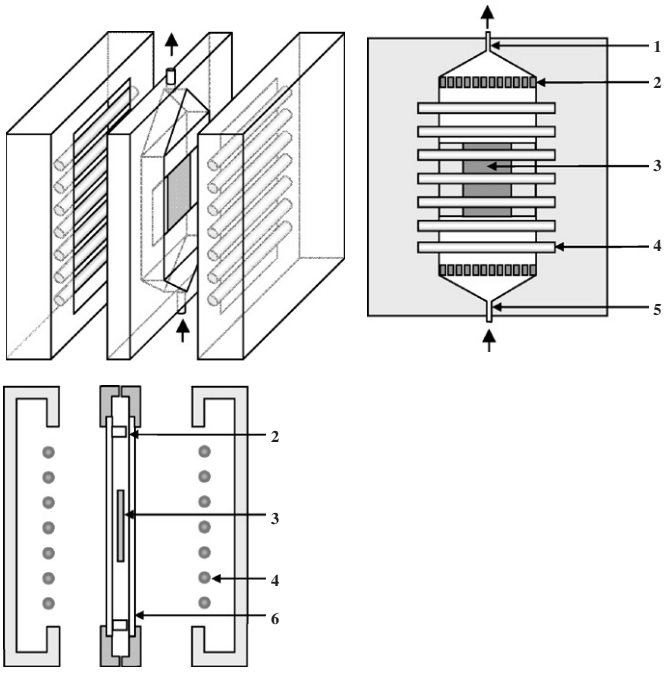

Fig. 3. Schematic representation of the laboratory photocatalytic reactor. Keys: (1) gas outlet, (2) flow homogenizer, (3) photocatalytic plate, (4) UV lamps, (5) gas inlet, and (6) acrylic windows.

Table 1
Laboratory photoreactor dimensions and characteristics

Description	Values
Lamp	$Z_L = 13.6$ cm; $R_L = 0.8$ cm; $P = 0.5$ W(∗), $\lambda =$ 300–420 nm
No. of lamps	7 + 7
Reactor flat plate	$x = 4.5$ cm; $z = 9$ cm
Reactive surface	81 cm^2

(∗) Total output power for a nominal input of 4 W.

In principle, the proposed averaged is needed if the radiation field and/or the catalyst immobilization on the flat plate is not uniform. The second problem was solved with the employed coating method. The first one has to be analyzed resorting to the radiative transfer equation.

Based on a reaction scheme (Fig. 4) proposed by Yamazaki and Araki (2002), an expression of the intrinsic reaction rate has been derived and verified by Imoberdorf et al. (2005). The following assumptions were considered by the authors: (i) the PCE degradation occurs through an elementary reaction involving the PCE attack by hydroxyl radicals followed by a sequence of steps that leads to the generation of a chlorine atom and a chain reaction initiated by the attack of the chlorine atom on the PCE, (ii) the PCE elimination through the first step of the chain propagation is much faster than that involving the direct hydroxyl radical attack (Amama et al., 2001; Zhao et al., 2002), (iii) the equivalent concept to the microsteady-state approximation (MSSA) in transient reactors may be applied to the net

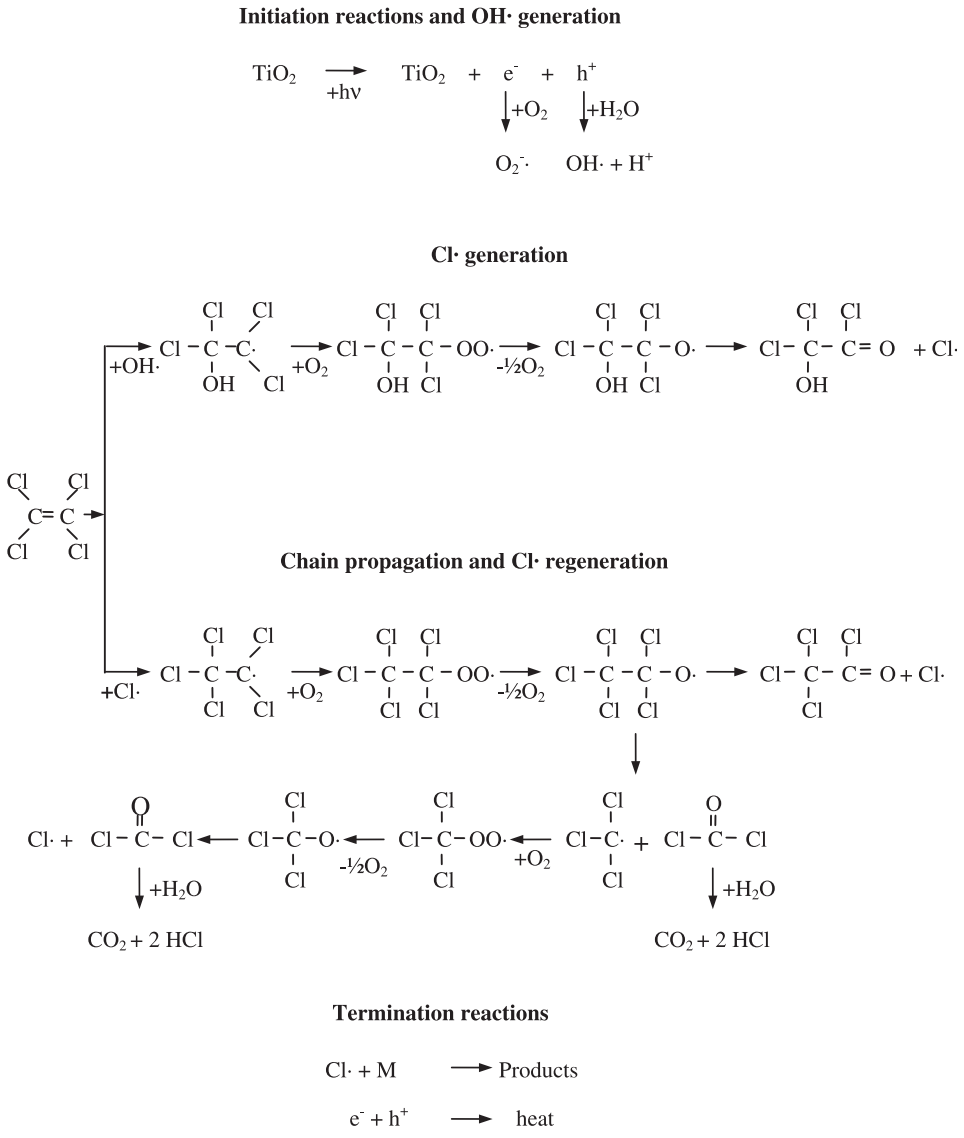

Fig. 4. PCE degradation reaction scheme.

generation rates of free radicals, atomic species, "free" electrons and holes, (iv) the termination reactions of the chlorine atomic species have been grouped in a single reaction (Sauer et al., 1995) between chlorine atoms and water vapor, other radical and atomic species, reactor walls, or other surfaces in the system, and (v) surface concentrations of adsorbed PCE and water can be related to gas phase concentrations through adsorption equilibrium constants. With these approximations, the following expression was obtained:

$$r_{\mathrm{PCE}} = -\frac{\alpha_1[\mathrm{PCE}]_{\mathrm{gas}}[\mathrm{H_2O}]_{\mathrm{gas}}}{(1 + K_{\mathrm{PCE}}[\mathrm{PCE}]_{\mathrm{gas}} + K_W[\mathrm{H_2O}]_{\mathrm{gas}})^2} \times \left(-1+\sqrt{\frac{1+K_{\mathrm{PCE}}[\mathrm{PCE}]_{\mathrm{gas}}+K_W[\mathrm{H_2O}]_{\mathrm{gas}}}{[\mathrm{H_2O}]_{\mathrm{gas}}}\alpha_2 r_g(\boldsymbol{x})+1}\right), \tag{3}$$

where the kinetic parameters α_1 and α_2 were defined by:

$$\alpha_1 = \frac{k_1k_2k_7K_{\mathrm{PCE}}K_W[\mathrm{Sites}]^2[\mathrm{O_2}]}{2k_{15}k_{16}[M]};$$

$$\alpha_2 = \frac{4k_{15}}{k_1k_2K_W[\mathrm{Sites}][\mathrm{O_2}]}. \tag{4}$$

Here K_{PCE} and K_W are the adsorption equilibrium constants of PCE and water, respectively, k_i (1 = 1, 2, 7, 15 and 16) are kinetic constants of the reaction scheme, [Sites] is the surface concentration of sites available for adsorption on the TiO_2 film, $[O_2]$ is the oxygen concentration, $[M]$ is the concentration of water, atomic or free radical species, reactor walls or other surfaces trapping atomic chlorine, and r_g is the superficial rate of electrons and holes generation.

The local superficial rate of electro–hole pair generation can be computed from the expression:

$$r_g(\boldsymbol{x}) = \overline{\Phi} \sum_{\lambda} e^{a,s}_{\lambda}(\boldsymbol{x}) = \overline{\Phi} e^{a,s}(\boldsymbol{x}), \tag{5}$$

where $\overline{\Phi}$ is the wavelength averaged primary quantum yield and $e^{a,s}_{\lambda}(\boldsymbol{x})$ the spectral local superficial rate of photon absorption (LSRPA) on the surface of the catalytic wall. Substituting Eq. (5) into Eq. (4) gives:

$$r_{\mathrm{PCE}} = -\frac{\alpha_1 [\mathrm{PCE}]_{\mathrm{gas}} [\mathrm{H_2O}]_{\mathrm{gas}}}{(1+K_{\mathrm{PCE}}[\mathrm{PCE}]_{\mathrm{gas}}+K_W[\mathrm{H_2O}]_{\mathrm{gas}})^2} \times \left(-1+\sqrt{\frac{1+K_{\mathrm{PCE}}[\mathrm{PCE}]_{\mathrm{gas}}+K_W[\mathrm{H_2O}]_{\mathrm{gas}}}{[\mathrm{H_2O}]_{\mathrm{gas}}}\alpha_2 \overline{\Phi} e^{a,s}(\boldsymbol{x})+1}\right). \tag{6}$$

Eq. (6) is of preeminent significance. From a plausible reaction sequence (Fig. 4) and reliable approximations, a local expression for the reaction kinetics in terms of observable independent variables has been obtained.

To solve Eq. (6) it is necessary to evaluate the LSRPA at each point on the TiO_2 films. To do this, the radiation coming from each group of UV lamps on either side of the photocatalytic plate should be considered. At each (x, z) position on the TiO_2 film, the spectral LSRPA can be evaluated by adding up the contributions to the local net fluxes corresponding to the radiation coming from each of the two sets of seven lamps (Fig. 5):

$$e^{a,s}_{\lambda}(x, z) = (q^{i}_{\mathrm{dir},\lambda} - q^{t}_{\mathrm{dir},\lambda}) + (q^{i}_{\mathrm{ind},\lambda} - q^{t}_{\mathrm{ind},\lambda}). \tag{7}$$

Here q^{i}_{λ} and q^{t}_{λ} are the incident and transmitted spectral net radiation fluxes, respectively. They are defined by the equation:

$$q_{\lambda}(x, z) = \boldsymbol{n}_G \cdot \boldsymbol{q}_{\lambda} = \int_{\Omega_L} I_{\lambda}(x, y, \boldsymbol{\Omega}) \boldsymbol{\Omega} \cdot \boldsymbol{n}_G \, \mathrm{d}\Omega, \tag{8}$$

where $\boldsymbol{n}_G$ is the outwardly directed unit normal to the film surface and $I_{\lambda}(x, z, \boldsymbol{\Omega})$ is the spectral radiation specific intensity. To solve this equation, the three dimensional source with superficial emission model (Cassano et al., 1995) and a ray tracing technique (Siegel and Howell, 2002) were used. The integration limits for the spherical coordinates θ and ϕ (corresponding to the definition of Ω_L) can be evaluated from the geometry and dimensions of the system and the UV lamp sets. In the radiation field model, the gas phase has been assumed transparent because air, PCE and water vapor do not absorb radiation in the wavelength range of the lamp emission. From the lamp model (diffuse and isotropic emission), according to the limiting values of the employed spherical coordinate system, the following boundary conditions result:

$$I_{\lambda}(r, z, \phi, \theta) = \begin{cases} 0, & (\phi, \theta) < (\phi_{\min,i}, \theta_{\min,i}), \\ I_{\lambda,L} = \frac{P_{\lambda,L}}{2\pi^2 R_L Z_L}, & (\phi_{\min,i}, \theta_{\min,i}) < (\phi, \theta) < (\phi_{\max,i}, \theta_{\max,i}), \\ 0 & (\phi_{\max,i}, \theta_{\max,i}) < (\phi, \theta), \end{cases} \tag{9}$$

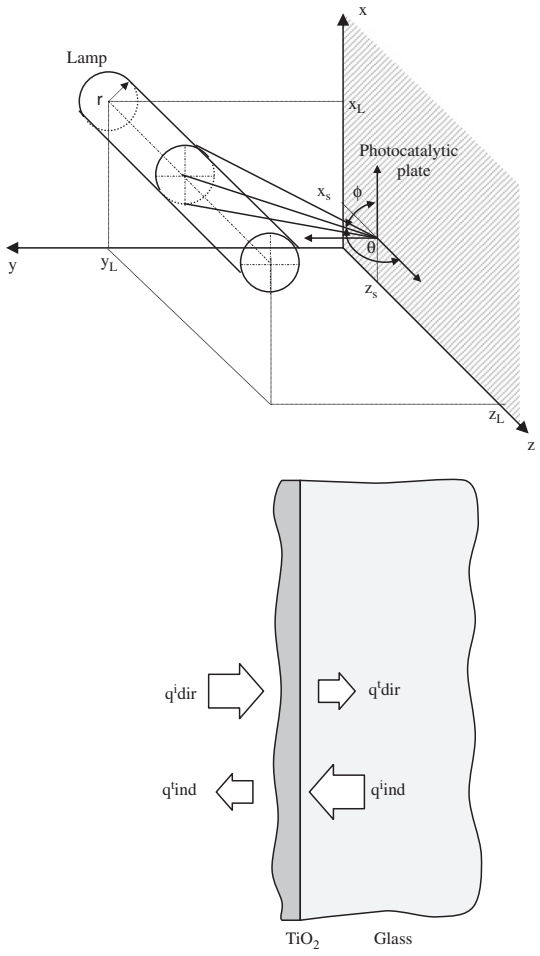

Fig. 5. Coordinate system for the radiation model of the laboratory photoreactor.

where $P_{\lambda,L}$ is the spectral emission power of the lamp, and R_L and Z_L are the radius and length of the lamp, respectively.

The final expression of the LSRPA at each point (x, y) on the thin catalytic film is

$$e^{a,s}(x, z) = \frac{P_{\lambda,L}}{2\pi^2 R_L Z_L} \sum_{\lambda} \sum_{\ell=1}^{7} \int_{\theta} \int_{\phi} \exp\left(-\frac{\kappa_{\lambda,a} e_a}{\cos\theta_n}\right) \times \left[1 - \exp\left(-\frac{\kappa_{\lambda,f} e_f}{\cos\theta_n}\right)\right] \sin^2\phi \sin\theta \, \mathrm{d}\phi \, \mathrm{d}\theta + \frac{P_{\lambda,L}}{2\pi^2 R_L Z_L} \sum_{\lambda} \sum_{\ell=8}^{14} \int_{\theta} \int_{\phi} \exp\left(-\frac{\kappa_{\lambda,a} e_a}{\cos\theta_n} - \frac{\kappa_{\lambda,g} e_g}{\cos\theta_n} - \frac{\kappa_{\lambda,f} e_f}{\cos\theta_n}\right) \times \left[1 - \exp\left(-\frac{\kappa_{\lambda,f} e_f}{\cos\theta_n}\right)\right] \sin^2\phi \sin\theta \, \mathrm{d}\phi \, \mathrm{d}\theta, \tag{10}$$

where $\kappa_{\lambda,a}$, $\kappa_{\lambda,f}$ and $\kappa_{\lambda,g}$ are the spectral absorption coefficients of the acrylic walls, the TiO_2 film and the glass plate, respectively; e_a, e_f, and e_g are the thickness of each media; and θ_n is the angle between the ray trajectory and the film outwardly directed normal.

Fig. 6 shows the predicted net radiation flux on the photocatalytic plate, employing an emitting system with one, two, three and seven black-light lamps. It should be noted that a higher radiation field uniformity at the center of the flat plate is obtained as the number of UV lamps is increased. Thus, for our experimental device with seven UV lamps, an inner rectangle (9×4.50 cm) can be identified where the difference between the maximum and minimum values of the net radiation flux is lower than 9%. This fact allowed us to consider a nearly uniform radiation flux over the TiO_2 film of the employed flat plate in the next section; i.e., for this particular reactor configuration, to consider that the system operates with a single value for $e^{a,s}$, derived form Eq. (10), but independent of position.

3.2. Evaluation of the kinetic parameters

In a previous work, Imoberdorf et al. (2005) found experimentally that the PCE reaction rate shows: (i) first-order kinetics with respect to the PCE concentration in the gas phase, (ii) linear dependence with respect to the irradiation level, and (iii) site-competitive kinetics for the dependence with the relative humidity. Consequently, the expression of the PCE reaction rate [Eq. (6)] can be simplified as follows:

$$r_{\mathrm{PCE}} = -\alpha \frac{[\mathrm{PCE}]_{\mathrm{gas}}}{1 + K_W [\mathrm{H_2O}]_{\mathrm{gas}}} e^{a,s}, \tag{11}$$

where the kinetic parameter α is

$$\alpha = \frac{\alpha_1 \alpha_2 \overline{\Phi}}{2} = \frac{k_7 K_{\mathrm{PCE}} [\mathrm{Sites}] \overline{\Phi}}{k_{16}[M]}. \tag{12}$$

Eqs. (11) and (12) can be combined with Eq. (10) to obtain the PCE reaction rate on the photocatalytic glass plate.

The kinetic parameters α and K_W were estimated from all the experimental data of the PCE reaction rate, applying a nonlinear regression procedure (Levenberg–Marquardt method). Table 2 gives the values of the two kinetic parameters and the corresponding confidence intervals. The quality of the obtained and, hopefully, intrinsic kinetic model can be seen when predicted and experimental PCE outlet conversions are compared in Fig. 7.

At this point we should look at the attributes of the obtained result. Since the laboratory reactor was operated at steady state under well mixed conditions, and the radiation flux was fairly uniform upon the surface of the catalytic plate, we have been able to considered that: (i) $[\mathrm{PCE}(x,z,t)] = [\mathrm{PCE}]$, (ii) $[\mathrm{H_2O}(x,z,t)] = [\mathrm{H_2O}]$ and (iii) $e^{a,s}(x,z) \cong \langle e^{a,s} \rangle_{A_R}$ [even if calculated with Eq. (9)]. This means that the whole laboratory reactor has been operating in each programmed run with a single value of PCE and water concentrations, as well as a single value of $e^{a,s}$. However the whole series of runs of the quoted work used to obtain the kinetic parameters was carried out changing the values of [PCE], $[\mathrm{H_2O}]$ and $e^{a,s}$. Therefore, Eq. (11) and the parameters in Table 2 are of general validity for reactors where the independent variables may be a function

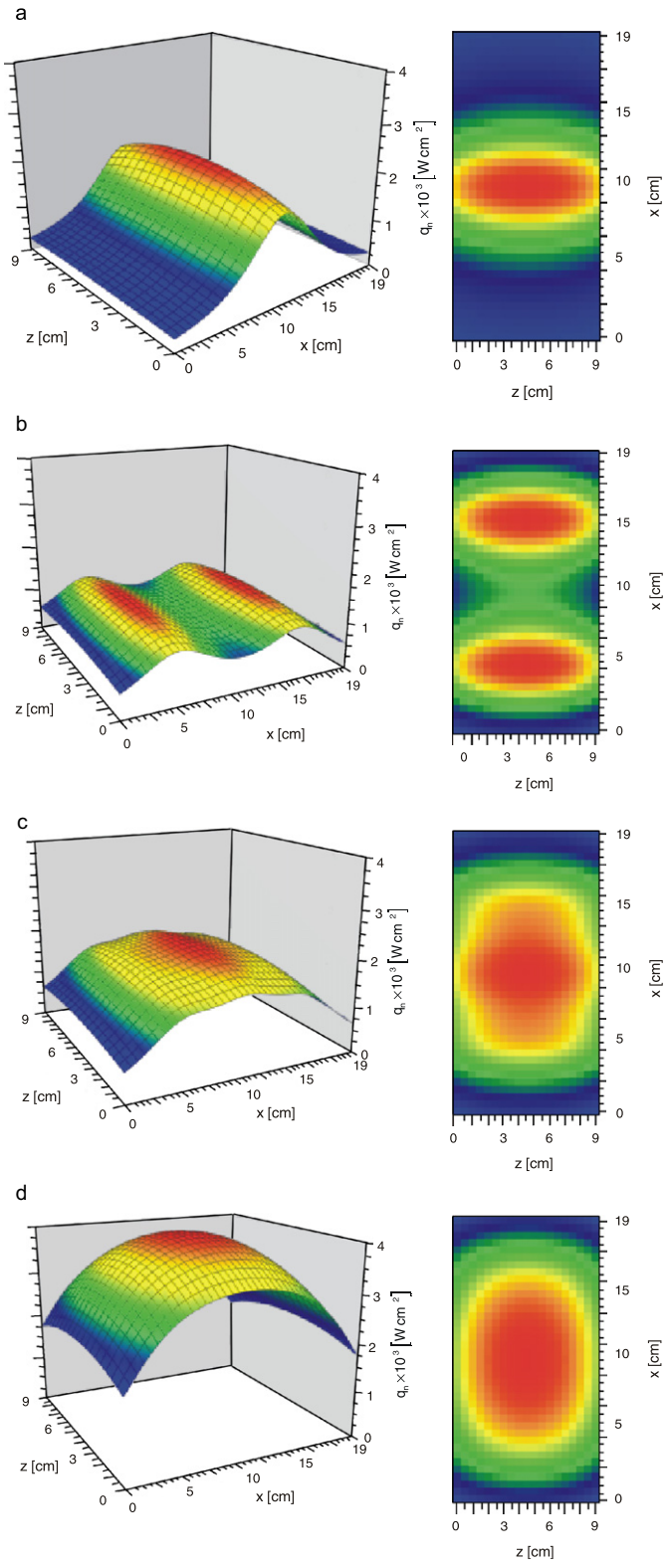

Fig. 6. 3-D predicted radiation fluxes on the photocatalytic plate: (a) 1 lamp, (b) 2 lamps, (c) 3 lamps, and (d) 7 lamps.

Table 2
Kinetic parameters and confidence intervals

Parameter	Value	95% Confidence interval	Units
α	1.54×10^{8}	0.19×10^{8}	$cm^3\,Einstein^{-1}$
K_w	3.21×10^{-4}	0.48×10^{-4}	$m^3\,mg^{-1}$

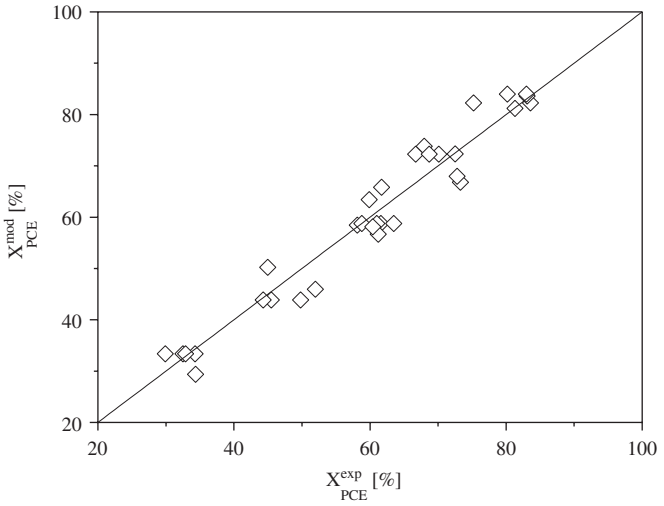

Fig. 7. Experimental and predicted outlet conversions for the laboratory photoreactor.

of position and/or time. Hence, we may equally write in more general terms, within the range of the explored variables, that:

$$r_{PCE}(\boldsymbol{x}, t) = -\alpha \frac{[PCE(\boldsymbol{x}, t)]_{gas}}{1 + K_W [H_2O(\boldsymbol{x}, t)]_{gas}} e^{a,s}(\boldsymbol{x}, t). \quad (13)$$

In other words, the achieved kinetic expression is valid for local and, eventually, time dependent values of the independent variables, a characteristic that was not shown in Eq. (11) because of the very specific type of reactor and the particularly chosen operating conditions. These characteristics were selected purposely to fulfill the condition stated before that the laboratory reactor must be as simple as possible and apt for a rigorous mathematical description. Eq. (13) should be equally valid for a batch, transient reactor or a continuous flow reactor. In other words, if in a different reactor configuration and operation, we can know through its corresponding mass and radiation balances, the local and/or temporal values of the PCE and water concentrations as well as the LSRPA, Eq. (13) will be rightfully applied to it. This is the key point in procedures of scaling-up from first principles. There is a single restriction in this statement: Eq. (11) was obtained working in a given range of irradiation rates and with a definite spectral distribution of the radiation output from the lamps. Under our operating conditions the linear dependence with the LSRPA and the [PCE] is an indication that for this particular system and the corresponding values of the different specific reaction rate constants, we were performing the reaction under comparatively low irradiation rates and low pollutant concentrations. At much higher values of $\sum_\lambda I^0_\lambda$ or [PCE] the prevailing mechanism could have rendered a different kinetic expression and, particularly the dependence with the LSRPA could have been different; typically, for example, the square root order for $e^{a,s}$ (Nimlos et al., 1993). Further, to perform the scale-up with a maximum of reliability it is necessary that the emission spectrum of the lamp/s used in the larger scale reactor be very similar to the ones corresponding to the lamps employed in the laboratory reactor. This is particularly so, because the kinetic model employs a wavelength averaged value for the primary quantum yield [Eq. (5)] that has an important dependence on the characteristics of the lamp emission spectrum.

In what follows we will apply these results to a very different reactor (shape and dimensions) and operating conditions. The irradiation rate will be of similar order of magnitude than before and the employed lamp has an almost identical wavelength emission characteristics.

4. Pilot scale photocatalytic reactor

4.1. Summary of reactor description and model

As it is sketched in Fig. 8, the reactor consists of four concentric cylindrical, borosilicate glass tubes which are transparent to UV radiation in most of the useful wavelength range (from 300 to 420 nm). A tubular UV lamp (Philips TL 18W/08 F4T5/BLB), was placed at the central axis of the system. The reactor dimensions are shown in Table 3. Reactants and products flow trough the annular spaces, entering the reactor by the outer annular space and exiting it by the inner one having a total available reaction length of 177 cm. The two walls directly in contact with the gas flowing through each annulus are coated with a thin layer of TiO_2. The inner and the outer tubes are covered only on the side in contact with the contaminated air stream. The thin layers of TiO_2 were deposited using the same sol–gel technique mentioned before in the description of the laboratory reactor. This is very important in order to have reproducible catalyst activity. The reactor was operated in the continuous mode, under isothermal conditions and at steady state. For more details the reader can refer to Imoberdorf et al. (2006).

According to the methodology described in Fig. 2, we need to know the new value of $e^{a,s}(\boldsymbol{x})$ that can be obtained applying the radiative transfer equation to the different reactor and a local evaluation of $[PCE(\boldsymbol{x})]$ from a position dependent mass balance. No time dependence was required because the reactor was run at steady state and the catalyst did not show any measurable lost of activity during the experiments.

The LSRPA was evaluated at each point on the catalytic surfaces, taking into account the incident radiation arriving from all possible directions coming out of the lamp surface in a diffuse and isotropic manner. The glass walls have good transmission properties in the wavelength range of interest but radiation absorption is not negligible. The model of the radiation field makes allowance for this effect.

Applying the radiative transfer equation, the local radiation flux at wavelength λ is given by Eq. (8). Clearly, in this case, the radiation field has angular symmetry and therefore the

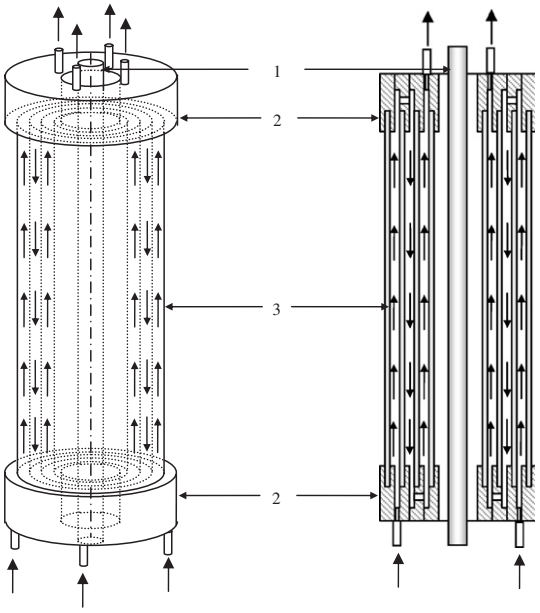

Fig. 8. Schematic representation of the pilot-scale photocatalytic reactor. Keys: (1) UV lamp, (2) distribution heads, and (3) borosilicate glass tubes.

Table 3
Pilot size photoreactor dimensions and characteristics

Description	Values
Lamp	$Z_L = 59\,\text{cm}$; $R_L = 1.4\,\text{cm}$; $P = 3.5\,\text{W}(*)$, $\lambda = 300$–$420\,\text{nm}$
No. of lamps	1
Reactor	$Z_R = 48\,\text{cm}$; $R_{R,\text{int}} = 1.48\,\text{cm}$; $R_{R,\text{ext}} = 4.26\,\text{cm}$
Annulus 1	$\chi_1 R_1 = 1.69\,\text{cm}$; $R_1 = 2.31\,\text{cm}$
Annulus 2	$\chi_2 R_2 = 2.51\,\text{cm}$; $R_2 = 3.30\,\text{cm}$
Annulus 3	$\chi_3 R_3 = 3.53\,\text{cm}$; $R_3 = 3.94\,\text{cm}$
Reactive surface	$5209\,\text{cm}^2$

(*) Total output power for a nominal input of 18 W.

local net radiation flux will only depend upon the (r, z) pair of cylindrical coordinates. Applying Eq. (8) with the adopted coordinate system (Fig. 9) we have for each point on the catalytic surface:

$$q_\lambda(r,z) = \int_\phi \int_\theta I_\lambda(r,z,\phi,\theta)\cos\,\phi\sin^2\theta\,\mathrm{d}\theta\,\mathrm{d}\phi. \tag{14}$$

In order to solve this equation we will use the three dimensional source with superficial emission model and the ray-tracing technique (Cassano et al., 1995; Siegel and Howell, 2002). The radiation beams coming directly from the lamp and arriving at a position (r, z) with directions given by the spherical coordinates (θ, ϕ), can only have been originated within the limits defined by the surface encompassing the three dimensional extension of the lamp as seen from the point of incidence.

At every position on the thin catalytic film, the LSRPA can be obtained from the local net fluxes resulting from all incident radiation beams coming from the lamp:

$$e_\lambda^{a,s}(r,z) = q_\lambda^i(r,z) - q_\lambda^t(r,z). \tag{15}$$

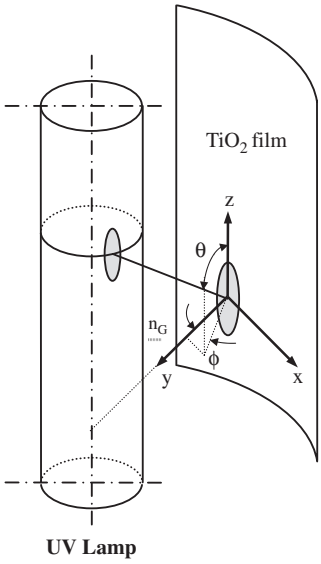

Fig. 9. Coordinate system for the radiation model of the pilot-scale photoreactor.

It must be remarked that even if Eqs. (7) and (15) have, conceptually, the same fundamental approach, in real terms there are very different. In this case radiation comes from one side only. Beside, Eq. (14), together with the limiting angles and boundary conditions (given by Eq. (9)) can be substituted into Eq. (15) and applied to the three annular spaces. Then, the final expression of the LSRPA at a given (r, z) position on a thin catalytic surface is

$$e^{a,s}(r,z) = \frac{P_{\lambda,L}}{2\pi^2 R_L Z_L} \sum_{\lambda=300\,\text{nm}}^{420\,\text{nm}} \int_{\phi_{\min}(r)}^{\phi_{\max}(r)} \int_{\theta_{\min}(r,z,\phi)}^{\theta_{\max}(r,z,\phi)} \times \exp\left(-n_g(r)\frac{\kappa_{\lambda,g}e_g}{\cos\alpha_n} - n_f(r)\frac{\kappa_{\lambda,f}e_f}{\cos\alpha_n}\right) \times \left[1 - \exp\left(-\frac{\kappa_{\lambda,f}e_f}{\cos\alpha_n}\right)\right]\cos\,\phi\sin^2\theta\,\mathrm{d}\theta\,\mathrm{d}\phi. \tag{16}$$

It should be specially noted the difference between Eqs. (16) and (10). This will be the first important change to introduce in Eq. (13). Moreover, differing from the specifically designed laboratory reactor, under no circumstances a uniform radiation absorption rate can be assumed for the catalytic surfaces existing in the multi-annular reactor.

With Eq. (16) inserted in Eq. (13) we have obtained a complete reaction kinetic expression to use in the mass balance corresponding to the pilot scale reactor. However, this is a continuous flow reactor and we will need information concerning the velocity field. The Reynolds number can be calculated for each annular space and, for the employed experimental conditions, its maximum value (in the inner annular space) was 25. Therefore, the reactor is operating under well defined laminar flow conditions. Assumption is made that end effects can be neglected (for a justification the reader is referred to Imoberdorf

et al., 2006) and the analytical solution for the annular space can be used. It is also clear that diffusive fluxes of PCE (the only species that experiments significant changes in concentration) cannot affect the velocity profile because of the very low contaminant concentrations. Hence, the fully developed velocity profile for a laminar flow of a Newtonian fluid through the jth annular duct is

$$V_{z,j}(r) = (-1)^{j+1}\frac{2Q}{\pi R_j^2}\frac{\ln\chi_j}{[(1-\chi_j^4)\ln\chi_j + (1-\chi_j^2)^2]} \times\left[1-\left(\frac{r}{R_j}\right)^2 - \frac{(1-\chi_j^2)}{\ln\chi_j}\ln\left(\frac{r}{R_j}\right)\right]; \quad (j=1,2,3), \tag{17}$$

where the upward direction was chosen as the positive one. Note that the momentum balance was not required in the laboratory reactor due to its particular operating conditions.

The mass transfer differential equation can be simplified with the usual assumptions, but in this case it must be considered that because the concentration of the more abundant species in the flowing gas mixture as well as its temperature are constant inside the reactor, the diffusivities of the species in the gas mixture are considered constant. Although always dilute, the only species that changes its concentration along the reactor in measurable percentages is PCE. Therefore, the radial diffusion can be considered as that of PCE in a more concentrated gas pseudo-component, namely air. This will be the governing mass transfer mechanism of PCE from the bulk of the gas stream to the catalytic boundaries and of the reaction products in the opposite direction. It was assumed that neither O_2 nor H_2O presents mass transfer limitations because these two reactants are in large excess with respect to PCE concentration. A second important consideration is that chemical reactions only take place on the photocatalytic film deposited on the annuli walls in contact with the flowing contaminated air stream or in its immediate vicinity. True homogeneous photochemical reactions are considered completely absent. Then the local mass balance can be written as

$$\frac{\partial C_{\mathrm{PCE}}(r,z)}{\partial z}V_{z,j}(r) = \frac{D^0_{\mathrm{PCE-Air}}}{r}\frac{\partial}{\partial r}\left(r\frac{\partial C_{\mathrm{PCE}}(r,z)}{\partial r}\right); \quad (0<z<Z_R;\ \chi_j R_j < r < R_j;\ j=1,2,3) \tag{18}$$

with the boundary conditions:

$$D^0_{\mathrm{PCE-Air}}\left.\frac{\partial C_{\mathrm{PCE}}(r,z)}{\partial r}\right|_{r=R_j} = r_{\mathrm{PCE}}[C_{\mathrm{PCE}}(R_j,z), C_{\mathrm{H_2O}}, e^{a,s}(R_j,z)]; \quad (0<z<Z_R;\ j=1,2,3), \tag{19}$$

$$D^0_{\mathrm{PCE-Air}}\left.\frac{\partial C_{\mathrm{PCE}}(r,z)}{\partial r}\right|_{r=\chi_j R_j} = -r_{\mathrm{PCE}}[C_{\mathrm{PCE}}(\chi_j R_j,z), C_{\mathrm{H_2O}}, e^{a,s}(\chi_j R_j,z)]; \quad (0<z<Z_R;\ j=1,2,3), \tag{20}$$

$$C_{\mathrm{PCE}}(r,z)|_{z=0} = C^0_{\mathrm{PCE}}; \quad (\chi_3 R_3 < r < R_3), \tag{21}$$

$$C_{\mathrm{PCE}}(r,z)|_{z=Z_R} = \frac{\int_{k_3R_3}^{R_3} C_{\mathrm{PCE}}(r,Z_R)V_{z,3}(r)r\,\mathrm{d}r}{\int_{k_3R_3}^{R_3} V_{z,3}(r)r\,\mathrm{d}r}; \quad (\chi_2 R_2 < r < R_2), \tag{22}$$

$$C_{\mathrm{PCE}}(r,z)|_{z=0} = \frac{\int_{k_2R_2}^{R_2} C_{\mathrm{PCE}}(r,0)V_{z,2}(r)\,\mathrm{d}r}{\int_{k_2R_2}^{R_2} V_{z,2}(r)r\,\mathrm{d}r}; \quad (\chi_1 R_1 < r < R_1), \tag{23}$$

where C_{PCE} is the PCE concentration, $D^0_{\mathrm{PCE-Air}}$ is the diffusion coefficient of PCE in air and r_{PCE} is the superficial reaction rate. The differences between the set of Eqs. from (18) to (23) when compared with Eq. (1) are manifestly evident. It is also important to recognize that in this mathematical modeling it can be clearly seen the nature of the catalytic wall reaction and its spatial dependence with respect to the position variables.

The PCE conversion at the reactor outlet is computed as follows:

$$X_{\mathrm{PCE}}[\%] = \left(1 - \frac{\int_{k_1R_1}^{R_1} C_{\mathrm{PCE}}(r,Z_R)V_{z,1}(r)r\,\mathrm{d}r}{C^0_{\mathrm{PCE}}\int_{k_1R_1}^{R_1} V_{z,1}(r)r\,\mathrm{d}r}\right)\times 100. \tag{24}$$

In Eq. (24) the concentrations must be obtained from the solution of the mass balance represented by Eqs. (18)–(23). In the boundary conditions, the reaction rates are obtained from Eq. (13) that was completed with the inclusion of Eq. (16). Finally, the velocity profiles are known from Eq. (17).

On the other hand, the experimental PCE conversion is evaluated by

$$X_{\mathrm{PCE}}[\%] = \frac{C^{\mathrm{in}}_{\mathrm{PCE}} - C^{\mathrm{out}}_{\mathrm{PCE}}}{C^{\mathrm{in}}_{\mathrm{PCE}}}\times 100. \tag{25}$$

5. Validation of the method

To substantiate the soundness of the proposed approach all what is needed is to compare results using Eq. (24) with those of Eq. (25). This has been done and is shown in Fig. 10. Predicted PCE conversions compared with experimental results show a root mean square error less than 5.6%. These results are very convincing, particularly because no adjustable parameters have been used in going from the laboratory reactor to the pilot scale one. It is also clear that the method has no restrictions to its application to bigger reactors. In fact, it is very difficult that a practical application will use annular spaces larger than the ones employed in the pilot scale prototype without introducing severe mass transfer limitations. Secondly, by analyzing results of the radiation model we conclude that it is not necessary to add more tubes to the multi-annular reactor, because almost no UV radiation is transmitted by the outer reactor tube. Thirdly,

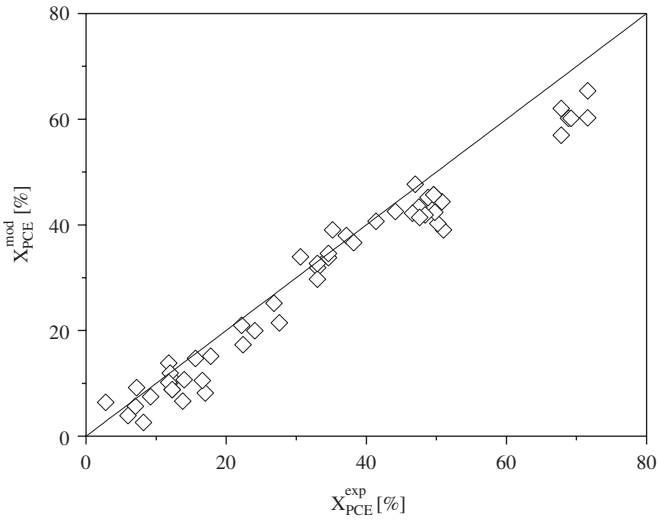

Fig. 10. Experimental and predicted outlet conversions for the pilot-scale photoreactor.

increasing the lamp output power per unit length of the tube will also bring forth diffusive limitations. Hence, the two most important changeable design variables are the flow rate (which is taken into account in the model with V_z) and the consequent change in the reactor length to achieve the desired conversion, which is explicitly accounted for with Z_R in all modeling equations. Lamps of the employed type, similar output power per unit length and identical emission wavelength distribution are commercially available in sizes up to 120 cm and with no very significant variations up to 220 cm (Actinic type). Its characteristics are taken into account in the modeling through the values of $P_{\lambda,L}$, R_L and Z_L.

6. Conclusions

A method has been described to scale-up photocatalytic reactors, with titanium dioxide immobilized on the reactor walls, directly from laboratory experiments. The procedure does not make use of adjustable parameters and predicts with good accuracy the performance of a pilot scale reactor. The approach is based exclusively in the fundamentals of chemical reaction and reactor engineering and radiation transport theory. This manner of proceeding opens the way to extend the technique to other type of photoreactor configurations.

Notation

A	area, cm^2
C	mass concentration, $mg\,m^{-3}$
D^0	molecular diffusivity, $cm^2\,s^{-1}$
e	thickness, cm
$e^{a,s}$	local superficial rate of photon absorption, Einstein $s^{-1}\,cm^{-2}$
I	specific radiation intensity, Einstein $s^{-1}\,cm^{-2}\,sr^{-1}$
k	kinetic parameter, units depend on the reaction step
K	equilibrium constant, $m^3\,mg^{-1}$
n	number of times that a radiation beam has been attenuated by each media, dimensionless
$\boldsymbol{n}_G$	outwardly directed unit normal to the catalytic film, dimensionless
P	emission power, W or Einstein s^{-1}
q	local net radiation flux, Einstein $s^{-1}\,cm^{-2}$
Q	volumetric flow rate, $cm^3\,s^{-1}$
r	reaction rate, $mol\,cm^{-2}\,s^{-1}$; also radial coordinate, cm
R	radius, cm
t	time, s
V_z	axial velocity, $cm\,s^{-1}$
x	cartesian coordinate, cm
X	conversion, dimensionless
y	cartesian coordinate, cm
z	axial coordinate, cm
Z	length, cm

Greek letters

α	kinetic parameter, $m^3\,Einstein^{-1}$
θ	spherical coordinate, rad
κ	volumetric absorption coefficient, cm^{-1}
λ	wavelength, nm
ϕ	spherical coordinate, rad
χ	internal/external radius ratio, dimensionless
Ω	solid angle, rad

Subscripts

λ	denotes wavelength
Air	relative to air
C	relative to cross-sectional area
f	relative to the TiO_2 film
g	relative to the electron-hole generation step; also relative to glass
gas	relative to gas phase
H_2O	relative to water
I	relative to the incident radiation
j	relative to the annular section (1 = inner, 2 = intermediate, 3 = outer)
L	relative to the UV lamp
M	relative to the element that participates in the radical inactivation
max	relative to the maximum limiting value
min	relative to the minimum limiting value
n	normal to the reaction area of the photocatalytic surface
PCE	relative to perchloroethylene
R	relative to the reaction; also relative to reactor

Superscripts

i	relative to the incident radiation flux
in	relative to the inlet stream
out	relative to the outlet stream
t	related to the transmitted radiation flux

Special symbols

$\langle \cdot \rangle$ means average value over a defined space
$[\cdot]$ means concentration

Acknowledgments

The authors are grateful to Universidad Nacional del Litoral (UNL), Consejo Nacional de Investigaciones Científicas y Técnicas (CONICET) and Agencia Nacional de Promoción Científica y Tecnológica (ANPCyT) for financial support. Thanks are also given to Eng. Gerardo Rintoul for his participation in some parts of the experimental work.

References

Amama, P.B., Itoh, K., Murabayashi, M., 2001. Photocatalytic oxidation of trichloroethylene in humidified atmosphere. Journal of Molecular Catalysis A: Chemical 176, 165–172.

Cassano, A.E., Martín, C.A., Brandi, R.J., Alfano, O.M., 1995. Photoreactor analysis and design: fundamentals and applications. Industrial & Engineering Chemical Research 34, 2155–2201.

Chang, C.P., Chen, J.N., Lu, M.C., Yang, H.Y., 2005. Photocatalytic oxidation of gaseous DMF using thin film TiO_2 photocatalyst. Chemosphere 58, 1071–1078.

Esterkin, C.R., Negro, A.C., Alfano, O.M., Cassano, A.E., 2005. Air pollution remediation. A fixed bed photocatalytic reactor made of glass fiber coated with TiO_2. A.I.Ch.E. Journal 51, 2298–2310.

Hall, R.J., Bendfeldt, P., Obee, T.N., Sangiovanni, J.J., 1998. Computational and experimental studies of UV/titania photocatalytic oxidation of VOCs in honeycomb monoliths. Journal of Advanced Oxidation Technologies 3, 243–252.

Hoffmann, M.R., Martin, S.T., Choi, W., Bahnemann, D.W., 1995. Environmental applications of semiconductor photocatalysis. Chemical Reviews 95, 69–96.

Hossain, M.M., Raupp, G.R., Hay, S.O., Obee, T.N., 1999. Three-dimensional developing flow model for photocatalytic monolith reactors. A.I.Ch.E. Journal 45, 1309–1321.

Ibrahim, H., De Lasa, H., 2004. Kinetic modeling of the photocatalytic degradation of air-borne pollutants. A.I.Ch.E. Journal 50, 1017–1027.

Imoberdorf, G.E., Irazoqui, H.A., Cassano, A.E., Alfano, O.M., 2005. Photocatalytic degradation of tetrachloroethylene in gas phase on TiO_2 films: a kinetic study. Industrial & Engineering Chemical Research 44, 6075–6085.

Imoberdorf, G.E., Irazoqui, H.A., Cassano, A.E., Alfano, O.M., 2006. Modeling of a multi-annular photocatalytic reactor for PCE degradation in air. A.I.Ch.E. Journal 52, 1814–1823.

Mohseni, M., 2005. Gas phase trichloroethylene (TCE) photooxidation and byproduct formation: photolysis vs titania/silica based photocatalysis. Chemosphere 59, 335–342.

Nicolella, C., Rovatti, M., 1998. Mathematical modelling of monolith reactors for photocatalytic oxidation of air contaminants. Chemical Engineering Journal 69, 119–126.

Nimlos, M.R., Jacoby, W.A., Blake, D.M., Milne, T.A., 1993. Direct mass spectrometric studies of the destruction of hazardous wastes. 2. Gas-phase photocatalytic oxidation of trichloroethylene over TiO_2: products and mechanisms. Environmental Science & Technology 24, 732–740.

Raupp, G.B., Nico, J.A., Annangi, S., Changrani, R., Annapragada, R., 1997. Two-flux radiation-field model for an annular packed-bed photocatalytic oxidation reactor. A.I.Ch.E. Journal 43, 792–801.

Sauer, M.L., Hale, M.A., Ollis, D.F., 1995. Heterogeneous photocatalytic oxidation of dilute toluene-chlorocarbon mixtures in air. Journal of Photochemistry and Photobiology A: Chemistry 88, 169–178.

Siegel, R., Howell, J.R., 2002. Thermal Radiation Heat Transfer. fourth ed. Hemisphere Publishing Corp., Bristol, PA.

Yamazaki, S., Araki, K., 2002. Photocatalytic degradation of tri- and tetrachloroethylene on porous TiO_2 pellets. Electrochemistry 70, 412–415.

Yamazaki-Nishida, S., Nagano, K.J., Phillips, L.A., Cervera-March, S., Anderson, M.A., 1993. Photocatalytic degradation of trichloroethylene in the gas phase using titanium dioxide pellets. Journal of Photochemistry and Photobiology A: Chemistry 70, 95–99.

Zhang, Z., Anderson, W.A., Moo-Young, M., 2003. Modeling of corrugated plate photocatalytic reactors and experimental validation. Chemical Engineering Science 58, 911–914.

Zhao, L., Ozaki, S., Itoh, K., Murabayashi, M., 2002. Self-catalytic behavior in gas-phase photocatalytic oxidation of trichloroethylene using TiO_2. Electrochemistry 70, 8–12.